Far-infrared magnetospectroscopy of polaron states in self-assembled InAs/GaAs quantum dots

S. Hameau, J. N. Isaia, Y. Guldner, E. Deleporte, O. Verzelen, R. Ferreira, and G. Bastard
Laboratoire de Physique de la Matière Condensée, Ecole Normale Supérieure, 24 rue Lhomond, 75231 Paris Cedex 05, France

J. Zeman
Grenoble High Magnetic Field Laboratory, CNRS/MPI, 25 avenue des Martyrs, 38042 Grenoble Cedex 9, France

J. M. Gérard
CNRS-Laboratoire de Photonique et Nanostructures, Boîte Postale 29, 92222 Bagneux Cedex, France

We investigate the far infrared magneto-optical transitions in self-assembled InAs quantum dots with different lateral diameters and we show that a purely electronic model is unable to account for the experimental data. We calculate the coupling between the mixed electron-LO-phonon states using the Fröhlich Hamiltonian, from which we determine the polaron states as well as the energies of the dipolar electric transitions. The excellent agreement between the experiments and the calculations obtained for the different samples provides strong evidence that the magneto-optical transitions arise between polaron states and that the electrons and LO phonons experience a strong coupling regime.

I. INTRODUCTION

The investigations of the confined states and of the electron-phonon coupling in self-assembled semiconductor quantum dots (QD's) have attracted recently considerable attention. InAs QD's that are lens-shaped hills spontaneously formed on a thin InAs wetting layer onto GaAs are particularly attractive because of their small and uniform size, their large areal density, and good confining properties. Semiconductor QD's, like artificial atoms, display discrete energy levels. The carriers bound to the QD's are, however, in interaction with phonons that display a continuum of finite width. The characteristic energy splitting of the InAs QD's electronic states (~ 50 meV) is comparable to the energy $\hbar \omega_{LO}$ of the longitudinal optical (LO) phonons and much larger than that of the longitudinal acoustical (LA) phonons. This has drastic consequences on the electron-phonon interaction in these nanostructures. First, it has been shown that the LA phonons are inefficient for the relaxation of the electron energy.[1] Second, because the LO phonons have very little energy dispersion, it has been suggested both theoretically[2] and experimentally[3] that electrons and LO phonons are in a strong coupling regime. The usual idea that an electron in an excited level can relax towards lower lying levels by irreversibly emitting one (or several) LO phonons when the energy separation matches $\hbar \omega_{LO}$, is wrong in QD's. In contrast to III-V bulk semiconductors or quantum-well structures where the electron-LO-phonon interaction corresponds to a weak coupling regime, electrons and LO phonons form mixed modes in QD's, the polaron states.

We had previously reported the first experimental evidence of this strong coupling regime using FIR (far infrared) magnetospectroscopy in a doped InAs QD's sample.[3] In the present paper, we report a systematic investigation of the electron-phonon interaction, using FIR magnetotransmission techniques up to $B = 28$ T at $T = 2$ K, in a series of selectively doped InAs QD's differing in lateral size. We study the

optical transitions between the ground and the first excited states that are *s*-like and *p*-like, respectively, in the quasicylindrical QD's. Depending on the FIR radiation polarization, two different transitions can be excited at $B = 0$, which evidences a size anisotropy of the QD's in the growth plane with a slight elongation along the $[1\bar{1}0]$ direction. The *B* dispersion of the transmission minima shows, in the whole magnetic-field range, drastic deviations with respect to the predictions of a purely electronic level model that incorporates both the orbital Zeeman splitting of the *p* states and the diamagnetic shifts of the bound levels. In particular, it evidences huge anticrossings when the energy splitting between the relevant electronic levels approaches $\hbar \omega_{LO}$ and $2\hbar \omega_{LO}$. As a model neglecting the electron-phonon coupling is definitively unable to account for the experimental data, we calculate the coupling between the mixed electron-lattice states using the Fröhlich Hamiltonian and we determine the polaron states and energies of the dipolar electric transitions. An excellent agreement between these calculations and the experimental data is obtained for all samples, demonstrating that the magneto-optical transitions occur between polaron states. Moreover, we have also calculated the time dependence of the survival probability for the various noninteracting electron-phonon states. Such probabilities are found to oscillate and never display a simple exponential decay like in bulk or quantum-well structures. This is another indication that electrons and LO phonons are always in a strong coupling regime in QD's.

II. EXPERIMENTAL DETAILS

The InAs/GaAs dots investigated here were grown on (001) GaAs substrates by molecular-beam epitaxy using the Stranski-Krastanov growth mode of InAs on GaAs.[4] As the resonant FIR absorption associated with a single layer of QD's is weak ($\sim 0.2\%$),[5] samples containing a multistack of 20 layers of InAs QD's were prepared in order to strengthen

TABLE I. Values of the major and minor axes a and b of the elliptical dot basis, and of the height h of the truncated cone, which best fit the FIR and PL measurements. R is the average radius.

Sample (nm)	I	II	III
a	11.4	11.4	10.7
b	10.2	9.8	9.8
$R=\sqrt{ab}$	10.8	10.6	10.2
h	1.8	2.4	2.4

this absorption. Two planes of dots were separated by a 50-nm-thick GaAs barrier. The density of QD's is $\sim 4 \times 10^{10}$ cm^{-2} for each plane, corresponding to an average center-to-center distance of 50 nm, large enough to neglect any interdot interactions. We can, therefore, reasonably consider our samples as constituted by isolated QD's. The shape of the InAs islands, estimated from transmission electron micrographs, is lenslike with a height of ~ 2 nm and a lateral diameter of ~ 20 nm. In the following, we discuss results obtained on three samples labeled (I), (II), and (III) differing in the lateral size of the QD's (see Table I). The lateral diameter decreases when going from (I) to (III) and, therefore, the electron confining energy increases. The gaps of the QD's were measured in the different samples by photoluminescence (PL) experiments at 2 K (the photoluminescence peak is centered at ~ 1.2 eV and the full width at half maximum is ~ 80 meV). The dots filling is realized by a delta doping of each GaAs barrier at 2 nm under the dots layer. The doping level $\sim 6 \times 10^{10}$ cm^{-2} was adjusted to transfer on average one electron per dot and populate only the ground state. We have investigated the optical transitions between the ground and the first excited states. Such transitions, which involve only conduction-band states, correspond to a resonance energy in the FIR. The sample transmission at 2 K was recorded by Fourier-transform spectroscopy in the FIR range 100–800 cm^{-1}. In order to eliminate the optical setup effects, the sample transmission was normalized to the substrate transmission. Two types of experiments have been performed with the radiation propagating perpendicular to the samples: transmission measurements at $B=0$ with a linearly polarized radiation and magnetotransmission measurements up to $B=28$ T at the Grenoble High Magnetic Field Laboratory using a resistive magnet and unpolarized radiation. The magnetic field was applied parallel to the growth (z) axis (Faraday configuration). Since the InAs QD's are flat objects, there is a quasidecoupling between the z and the lateral electron motions. The FIR experiments with the radiation electric field along the InAs planes probe essentially the lateral degree of freedom of the bound electrons and are thus sensitive to the lateral homogeneity of the QD's. Figure 1 shows typical transmission spectra obtained at $B=0$ on samples (II) and (III). The strong intensity of the observed resonances ($\sim 9\%$) as well as the sharpness of the lines [the full width at half maximum (FWHM) is ~ 4 meV] evidences the good quality of this sample. Very similar results are obtained for the other samples. The absorption probability for the observed s-p resonance can be estimated from a simple model detailed in Appendix A. We find that, for a single plane con-
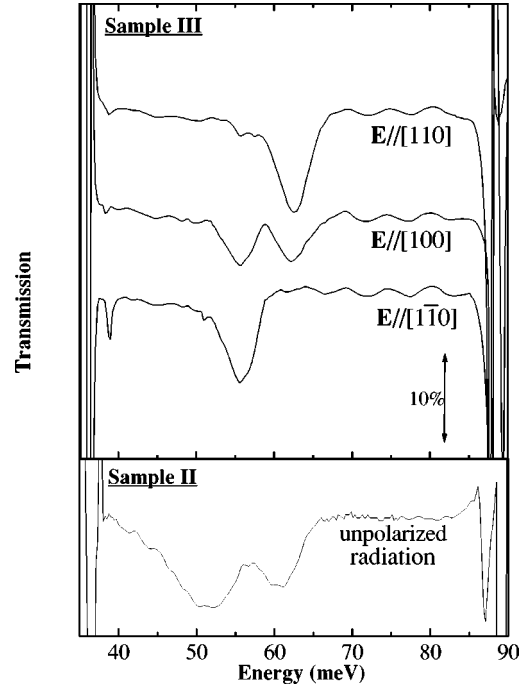
FIG. 1. Transmission spectra at $B=0$ and $T=5$ K of sample (III) for radiation linearly polarized along the [110], [1$\bar{1}$0], and [100] directions and of sample (II) for an unpolarized radiation.

taining $\sim 4 \times 10^{10}$ cm^{-2} QD's with one electron per dot, the absorption amplitude using a FWHM of 4 meV is 0.44%. This result accounts well for the experimental data in our samples consisting of 20 QD's layers and shows that the absorption is consistent with a dot population of one electron.

III. RESULTS

For QD's with a perfect cylindrical symmetry, the electronic eigenstates are of the form

$$\psi(\rho,\theta,z)=e^{im\theta}g_m(\rho,z), \quad L_z|\psi\rangle=m\hbar|\psi\rangle, \qquad (1)$$

where (ρ,θ) are the polar coordinates in the QD's plane, $L_z=-i\hbar\partial/\partial\theta$ is the angular momentum projection along the growth axis (z), and m is an integer. The states are labeled $s(m=0)$, $p_\pm(m=\pm 1)$, $d_\pm(m=\pm 2),\dots$, so that the ground and the first excited states are s-like and p-like, respectively. One should add one more quantum number to account for the different z motions but the actual InAs QD's are sufficiently flat to accommodate a single bound state when $m=0,\pm 1$. The two excited $p_\pm$ states would be degenerate at $B=0$ for a cylindrical symmetry, so that a single s-p transition would be expected. In fact, in all investigated samples, the s-p absorption at $B=0$ consists of two components as shown in Fig. 1 for samples (II) and (III). In sample (III), for radiation linearly polarized along the [110] direction, a single line is excited at 63 meV while a different single line is measured at 56 meV for polarization along [1$\bar{1}$0]. Both lines are observed with comparable intensities for the intermediate polarization along [100], or for unpolarized radiation. An anisotropy in the dots shape, an inhomo-

(a)   **(b)**
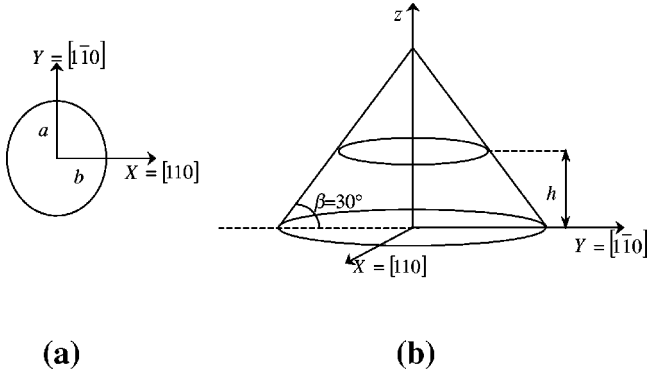
FIG. 2. Electronic levels of QD's are calculated by using the following geometrical model for the quantum dots : (a) the dot basis is supposed to be elliptical with major and minor axes a and b, respectively, (b) the quantum dot is modeled by a truncated cone of height h and basis angle $\beta = 30°$.

geneous electric field, or more generally a perturbation of the form $\omega(\rho, \theta)$ that involves components with d symmetry, can cause such a splitting between the two components. Taking into account previous works,[5–7] it is likely that the slight elongation of the InAs dots along the direction [1$\bar{1}$0] is responsible for this splitting. The fact that the absorption is totally polarized along the [110] and [1$\bar{1}$0] axes in samples containing many dots proves that the anisotropy axes are not oriented at random from one dot to another, but that they are genuine features of the growth of any QD. It is possible to account for the measured anisotropy by assuming that the dot basis is not circular but elliptical with major and minor axes a and b, respectively [Fig. 2(a)]. By using a variational procedure with Gaussian functions, we have calculated the electronic levels of QD's modeled by a truncated cone of height h and basis angle $\beta = 30°$ [Fig. 2(b)] as estimated from transmission electron micrographs. Note that scanning tunneling microscopy of similar samples[8] confirms this geometrical shape of the dots. The potential of the elliptical dot reads $V = V_0 + \delta V$, where V_0 is the cylindrical dot potential and $\delta V / V_0 \ll 1$ describes the slight anisotropy. The electron effective mass m^* is determined from the orbital Zeeman effect as described in Sec. IV. The exact composition of the QD's is not known but it is clear that a significant interdiffusion occurs between the InAs layers and the GaAs barriers. The importance of this intermixing has been recently pointed out by Stark effect spectroscopy.[9] For the sake of simplicity, we have considered in the calculations a homogeneous gallium content of 30% in the QD's,[10] resulting in a conduction-band offset of 488 meV. Finally, the parameters a, b, and h that best fit the FIR and PL measurements are listed in Table I for the different samples. The $\sim 10–15$ % anisotropy in the growth plane is found in good agreement with previously reported observations.[5–7] Samples (I) to (III) correspond to a decreasing average QD radius $R = \sqrt{ab}$.

In the presence of a magnetic field B applied parallel to the growth axis, the electronic Hamiltonian is given by

$$H_e = \frac{\mathbf{P}^2}{2m^*} + V(\rho, \theta, z) + \frac{1}{2}\omega_c L_z + \frac{1}{2}m^*\left(\frac{\omega_c}{2}\right)^2\rho^2, \quad (2)$$

where $\mathbf{P}$ is the electron momentum and $\omega_c = eB/m^*$. The two magnetic-field-dependent terms in Eq. (2) correspond to the linear and quadratic Zeeman effects. The larger one is the linear Zeeman effect, which affects only $m \neq 0$ states and splits the $\pm m$ states. The quadratic Zeeman term gives diamagnetic shifts that do not exceed 10 meV in the investigated field range. For a purely electronic problem that includes the small in-plane anisotropy δV of the confining potential, one expects to observe two transitions with energies $\hbar\omega_\pm$,

$$\hbar\omega_\pm = E_0 \pm \frac{1}{2}\sqrt{\delta^2 + \hbar^2\omega_c^2} + \gamma B^2, \quad (3)$$

where δ is the zero-field splitting of the excited $p_\pm$ states and the last term corresponds to the quadratic Zeeman effect. The two high-field asymptotes $E_0 \pm \hbar\omega_c/2 + \gamma B^2$ correspond to the orbital Zeeman splitting of the $p_\pm$ states. Let us first focus on sample (II). Figure 3(a) displays the magnetotransmission spectra recorded at $T = 2$ K on sample (II) between $B = 9$ and $B = 28$ T. Two main absorption regions are observed (at 40–50 meV and 65–85 meV), whose energy splitting is found to increase with B because of the orbital Zeeman effect of the p states. Depending on the magnetic field, four different resonance lines are observed whose minima are indicated by the dashed lines. The zero-transmission region around 35 meV corresponds to the reststrahlen band of the GaAs substrate, while that around 90 meV arises from the absorption of the setup windows. A quite similar behavior is observed in the other samples. The B dispersion of the resonances consists in four branches as shown in Fig. 3(b) (full circles). It is clear that the transition energies cannot be accounted by the simple expression given in equation Eq. (3). For instance the solid lines in Fig. 3(b) show the calculated dispersion using $E_0 = 55.5$ meV, $\delta = 9.5$ meV, $\gamma = 4.10^{-3}$ meV T^{-2}, and $m^* = 0.07 m_0$ (these values will be discussed later). Striking anomalies are observed. First, two anticrossings appears around 70 meV and 80 meV. Second, the dispersion of the lowest branch considerably deviates from its expected behavior in the whole B range. The anticrossing at ~ 70 meV occurs at an energy that is about twice the energy $\hbar\omega_{LO}$ of a LO phonon either in GaAs or in InAs strained to GaAs.[11] As shown in Fig. 3(a) and Fig. 3(b), an additional absorption line appears at $B = 9$ T whose magnitude increases with B so that a doublet is observed in the field range 9–22 T. A similar doublet is observed around 25 T when the energy difference between p_+ and p_- is equal to $\hbar\omega_{LO}$. Finally, the strong departure of the lowest branch from the predicted behavior indicates a pinning of this branch close to $\hbar\omega_{LO}$ for $B > 20$ T.

These anomalies, observed for all samples as shown in Fig. 4 (full circles), resemble the well-known resonant magneto-polaron effects observed in the dispersion of magneto-optical transitions in III-V bulk materials or quantum-well structures. At the magnetic field for which the cyclotron energy is equal to $\hbar\omega_{LO}$, a small deviation of the transition energy as well as an anticrossing occur.[12–14] However, while such anomalies are only observed within a narrow magnetic-field region in bulk material (< 1 T), they oc-
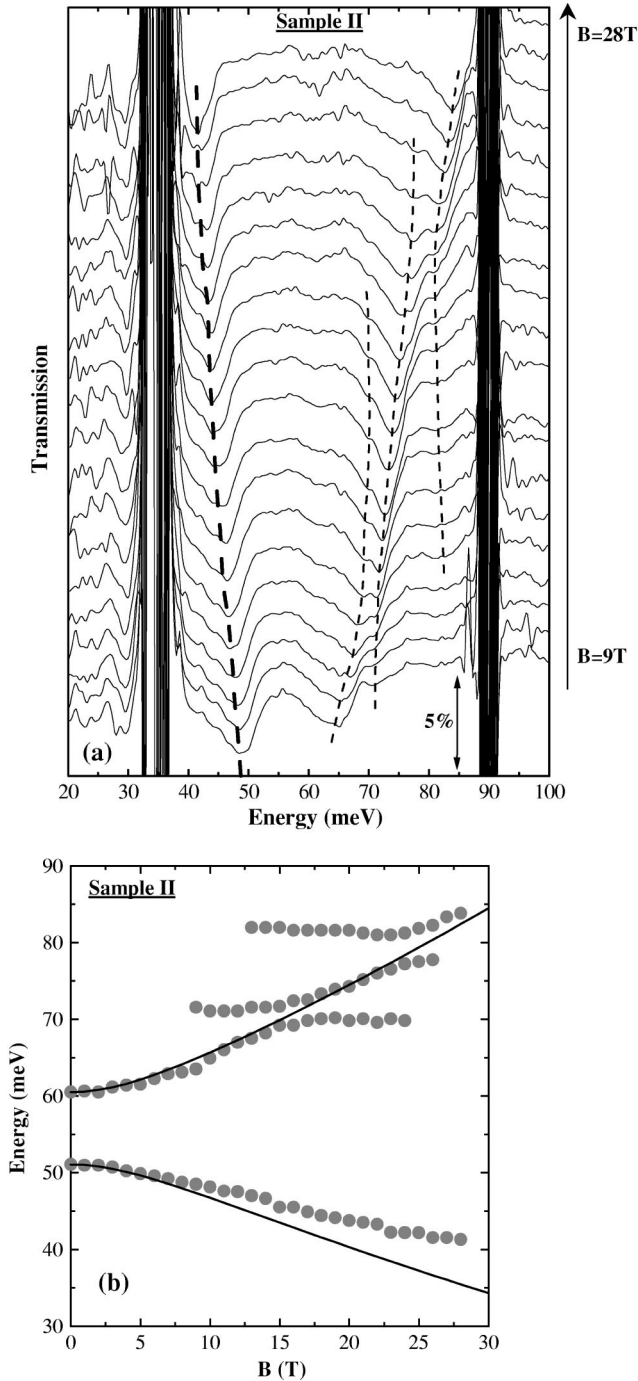
FIG. 3. (a) Magnetotransmission spectra recorded at $T = 2$ K on sample (II) between $B = 9$ and $B = 28$ T. Traces have been offset for clarity. Four different resonance lines are observed whose minima are indicated by the dashed lines. (b) Magnetic-field dispersion of the resonances (full circles) for sample (II). The solid lines are the calculated dispersions from Eq. (3) using the parameters listed in the text.

cur in the whole investigated B range in the QD's as shown in Figs. 4(a)–4(c) for the (I), (II), and (III) samples, respectively. Also, the magnitudes of the anticrossings are much larger than those in bulk or quantum-well structures. Finally, we are not aware that a two phonon resonant magnetopo-

laron has ever been evidenced in bulk III-V materials. One is, therefore, led to the conclusion that there exists strong resonant magneto-polaron effects in QD's when the energy difference between two confined electronic states is equal to a multiple of $\hbar\omega_{LO}$. Figure 5 displays a scheme of the energies of the noninteracting electron-phonon states $|\nu,n\rangle$, with $\nu = s$ or $p_{\pm}$ and $n = 0,1,2$ represents the n LO-phonon states, for the various samples in the B range used in our study. In these diagrams, one has used the zero-field s-p energy separation from the FIR results and $m^* = 0.07\,m_0$. The ground state $|s,0\rangle$ is taken as the energy origin and the quadratic shifts of the levels are neglected. The solid lines represent the discrete levels, while the gray lines are the narrow continuum levels with one or two LO phonons. It is clear in Fig. 5 that the magnetic field can tune a resonant interaction between the discrete $|p_{\pm},0\rangle$ states and the continuums $|s,1\rangle$, $|p_-,1\rangle$, and $|s,2\rangle$. One can check for each sample the one-to-one relationship between the crossovers of the various noninteracting levels in Fig. 5 and the observed deviations and anticrossings shown in Fig. 4. In particular, it is clear in samples (II) and (III) [Fig. 4(b) and Fig. 4(c)] that a small anticrossing (2–3 meV) first occurs corresponding to a two LO-phonon polaron and then a larger one (5 meV) associated to a single LO-phonon polaron takes place at higher magnetic field. Because of the particular level arrangement in sample (I) where the zero-field s-p energy separation is closer to $\hbar\omega_{LO}$ (see Fig. 5), the opposite situation occurs as shown in Fig. 4(a).

IV. ANALYSIS AND DISCUSSION

Because a purely electronic level model is unable to account for the experimental data, we have to consider FIR magneto-optical transitions between polaron states and, therefore, to calculate the coupling between the relevant mixed electron-phonon states. In bulk materials, it is well known that one has to diagonalize the Fröhlich Hamiltonian that describes the Coulomb interaction between a moving electron and the dipoles vibrating at the angular frequency ω_{LO} corresponding to a longitudinal optical mode. It is associated with the partial ionicity of the bonds between the two different atoms that constitute the III-V semiconductors. In QD's, the phonon spectra are not known accurately as a result of the uncertainties on the shape and composition of the actual dots. The notion of longitudinal and transverse modes is most likely not as strict in a dot as in bulk GaAs. Moreover, there should exist interface phonon modes. All these uncertainties result in severe difficulties in establishing what would be the equivalent of the Fröhlich term in an actual QD (see Ref. 15 for a spherical dot). On the other hand, an actual InAs island comprises several thousands of unit cells, and thus should have a quasibulk phonon spectrum. Like in III-V bulks, each anion is surrounded by four cations with a slightly polar bond between them. Therefore, the basic ingredients of the Fröhlich Hamiltonian are maintained in actual dots, with oscillating dipoles interacting with a moving charge. These considerations have led us to take a bulklike Fröhlich Hamiltonian to describe the interaction between an electron bound to a dot and the optical phonon
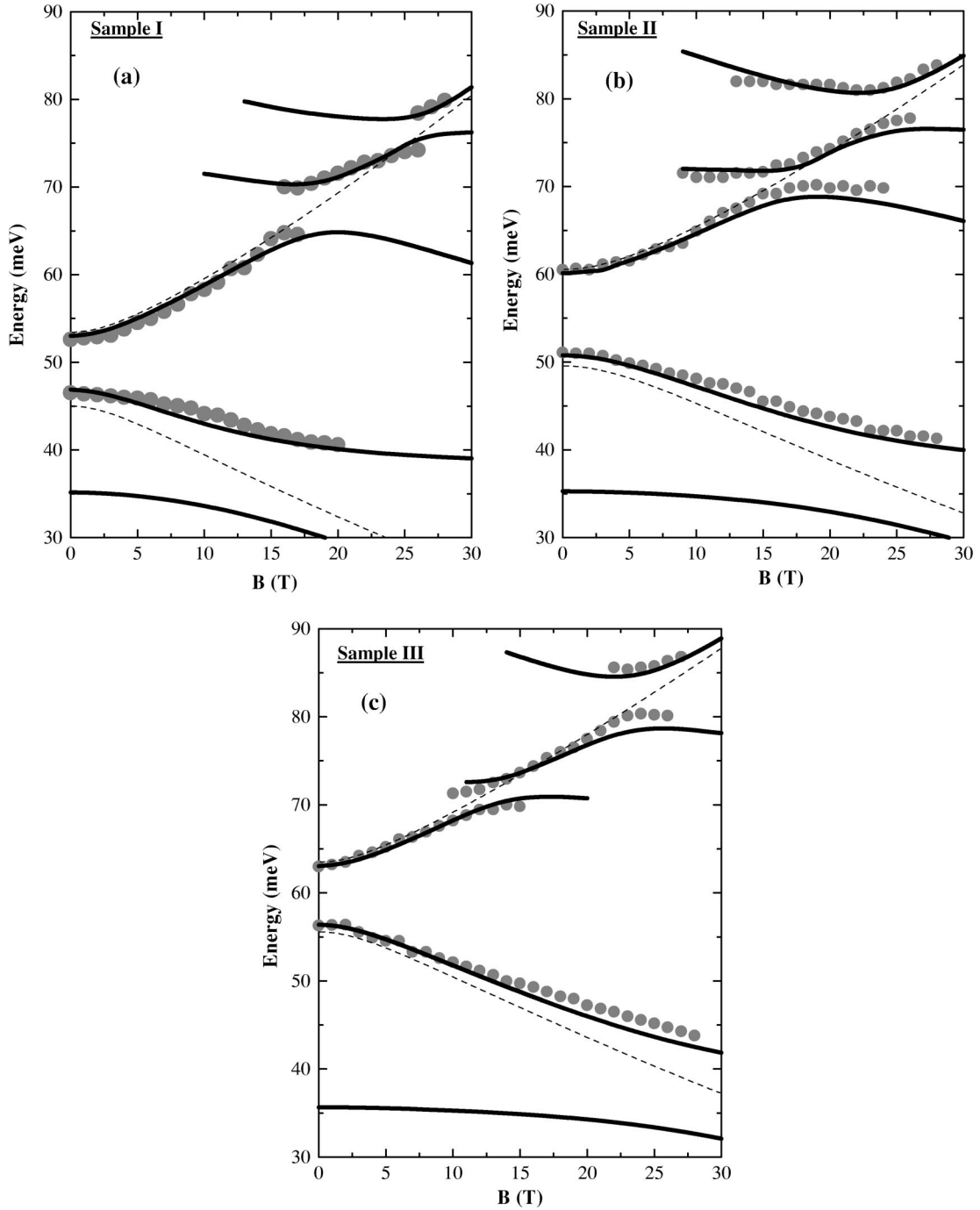
FIG. 4. Magnetic-field dispersion of the resonances (full circles) for (a) sample (I), (b) sample (II), (c) sample (III). In the three figures, the bold solid lines are the resonances dispersions calculated from the numerical diagonalization of the Hamiltonian including the Fröhlich term, using the parameters listed in the text. The dashed lines are the calculated resonance dispersions by suppressing the electron-phonon coupling for the same parameters as previously.

modes of the structure. The dimensionless Fröhlich constant α characterizes the ionicity of the material and the intensity of the coupling. We have taken the coupling constant α in QD's as an adjustable parameter since it has already been reported that α could be enhanced in dots as compared to the bulk situation.[16]

The numerical diagonalization of the Hamiltonian including the Fröhlich term gives the polaron states. The noninter-

acting mixed states are labeled $|\nu, n_{\{\mathbf{q}\}}\rangle$ where $|\nu\rangle = |s\rangle$, $|p_\pm\rangle$ are purely electronic states (in what follows $p_\pm$ denotes the two electronic levels that result from the two excited states admixed by the anisotropy term). $|n_{\{\mathbf{q}\}}\rangle$ denotes the ensemble of n LO-phonon states in the $\{\mathbf{q}\}$ modes. The basis used in the numerical diagonalization consists of $|s,0\rangle$, $|s,1_{\mathbf{q}}\rangle$, $|p_-,0\rangle$, $|p_+,0\rangle$, $|p_-,1_{\mathbf{q}}\rangle$, $|p_+,1_{\mathbf{q}}\rangle$, $|s,2_{\mathbf{qq'}}\rangle$ (see Fig. 5). Moreover, the interaction with $|p_-,2_{\mathbf{qq'}}\rangle$ and
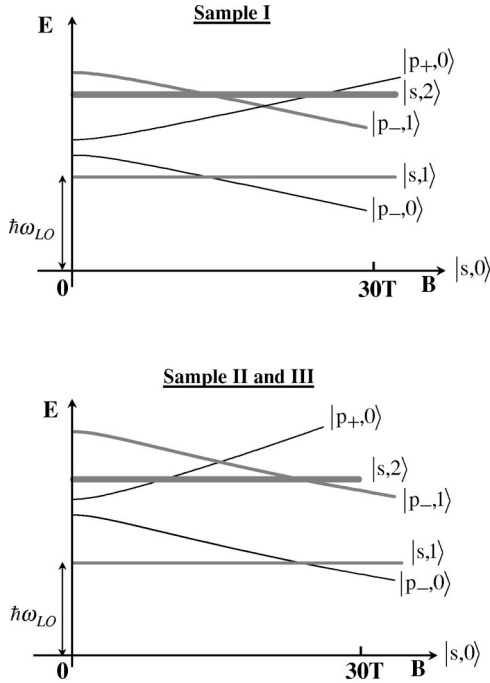
FIG. 5. Scheme of the energies of the noninteracting electron-phonon states for the various samples for B varying from 0 to 30 T. The pure electronic states are represented by black solid lines. The continuum with one or two LO phonons are represented by gray lines symbolizing the continuum width.

$|s,3_{\mathbf{qq'q''}}\rangle$ are introduced perturbatively. Note that electron-phonon states that differ by two phonons are not coupled at the lowest order by the Fröhlich Hamiltonian that is linear in the LO-phonon destruction and creation operators $a_{\mathbf{q}}$ and $a_{\mathbf{q}}^{+}$.[17] The two phonon polarons correspond, therefore, to an indirect interaction between $|s,2_{\mathbf{qq'}}\rangle$ and $|p_{+},0\rangle$. The LO-phonon dispersion $\omega_{LO}(\mathbf{q})$ was taken into account as follows. We took $N=56$ values for the wave vector $\mathbf{q}$ close from the center of the Brillouin zone (we have checked that retaining $N=80$ values leads to the same results, this is because the Fröhlich interaction favors small wave vectors). The largest q value was such that any matrix element for yet larger q values was less than 1% of its largest value. This reduces the effective energy width of the one and two phonon continuums to about 0.4 meV and 0.8 meV, respectively (whereas the energy width of the one phonon continuum corresponding to the whole first Brillouin zone is ~ 6 meV).

The numerical diagonalization produces many mixed electron-phonon, or polaron states. Most of them are irrelevant for the magneto-optical data. In fact, these experiments probe the polaron levels through their electronic components since one actually measures the light absorption that results from an electric dipole transition. Since the ground polaron state is mostly built from the unadmixed $|s,0\rangle$ state, the FIR experiments provide information on the projection of the excited polaron states on $|p_{+},0\rangle$ and $|p_{-},0\rangle$ states. We have, therefore, only retained the polaron levels with square projections on $|p_{+},0\rangle$ and $|p_{-},0\rangle$ larger than 10%, which corresponds roughly to the experimental sensivity, in order to obtain the magneto-optical transition energies. The bold solid

curves of Figs. 4(a)–4(c) are the resonance dispersions calculated for $\alpha=0.075$, $m^{*}=0.07\,m_{0}$, $\hbar\omega_{LO}=36$ meV, taking $\delta=7,10,7$ meV and an average zero-field s-p energy separation of 48, 54, and 58.5 meV for samples (I), (II), and (III), respectively. The field and energy positions as well as the magnitude of the various anticrossings are very well described by our model. The excellent agreement obtained for all samples demonstrates that the magneto-optical transitions occur between polaron states. The first predicted branch at 30–35 meV is not observed experimentally because it is too near to the reststrahlen band of the GaAs substrate. The parameters m^{*} and $\hbar\omega_{LO}$ of the QD's samples are comparable to those of bulk GaAs. The effective mass, which is roughly the same for the three samples, is considerably heavier than in pure bulk InAs but it is reasonably consistent with the ~ 1.2 eV gap measured by PL in our QD's. Taking into account the effects of strain, interdiffusion, and band nonparabolicity, due to the carrier confinement, brings the mass of In(Ga)As QD's not far from that of bulk GaAs. Note also that m^{*} is consistent with previous experimental determinations.[5] The Fröhlich constant α is slightly larger than in bulk InAs or GaAs (25% larger than in bulk GaAs), in agreement with previous findings.[15,16] There is a clear hierarchy between the measured anticrossings. For the one phonon polarons, the anticrossings are the larger when the electron part of the uncoupled electron-phonon states have the smaller difference in the projection of their angular momentum along z: the s-p_{-} anticrossing is larger than the p_{+}-p_{-} one (see Fig. 4). This trend is in agreement with the predictions one can make from the diagonalization of a bulk-like Fröhlich Hamiltonian in a quantum dot. The two phonon polarons display less repulsion at resonance than one phonon polarons, which is also well accounted for by our Fröhlich-like model.

The dashed lines in Figs. 4(a)–4(c) are the calculated resonance dispersions by suppressing the electron-phonon coupling (i.e., by putting $\alpha=0$ in the calculations). For each magnetic field, the difference between the solid and dashed lines shows the electron-phonon interaction contribution. It is noteworthy that a polaron effect occurs in the whole B range from $B=0$ to 28 T, showing again that the magneto-optical transitions always occur between polaron states. The contribution at $B=0$ depends on the position of the s-p energy as compared to $\hbar\omega_{LO}$. The weaker is the s-p separation, the larger is the correction at $B=0$. This last point is clearly observed in Fig. 4 when comparing samples (I) and (III).

In order to understand the origin and the amplitude of the various anticrossings, especially of the two anticrossings at 70–80 meV, we have developed a simple model that involves dispersionless LO phonons. Since the numerical diagonalization of the Fröhlich Hamiltonian involves small phonon wave vectors and thus uses a very small part of the phonon dispersion (we have seen that the effective energy width of the one LO-phonon continuum is ~ 0.4 meV), the dispersionless phonon model will give good results if the amplitude of the anticrossings is much larger than the continuum width. First, consider the deviation around 40 meV. This deviation originates from the interaction between the

(a)

(b)
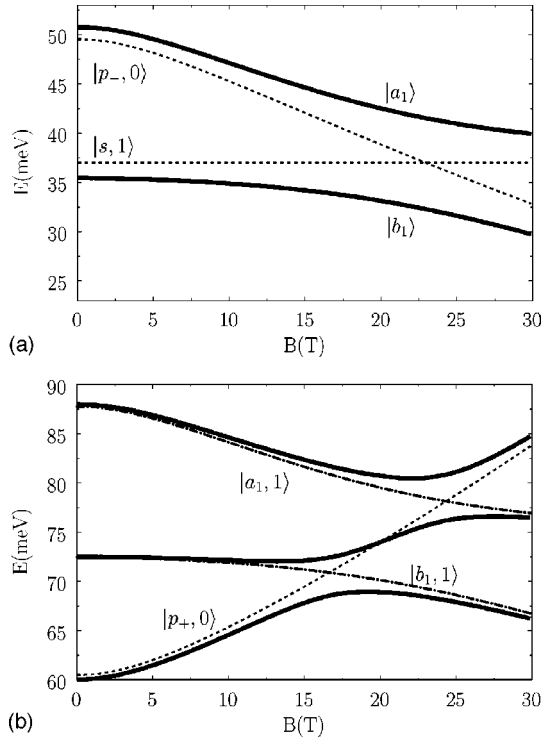
FIG. 6. Calculated polaron energies in the framework of a dispersionless LO-phonon model for sample (II). (a) Dashed lines: noninteracting electron-phonon states $|p_-,0\rangle$ and $|s,1\rangle$; solid lines: the two discrete polarons $|a_1\rangle$ and $|b_1\rangle$. (b) Dashed-dotted lines: the two flat polaron continuums $|a_1,1\rangle$ and $|b_1,1\rangle$, which are the same as in Fig. 6(a) shifted by $\hbar\omega_{LO}$; dashed line: noninteracting electron-phonon state $|p_+,0\rangle$; solid lines: the three states resulting from the interaction between $|a_1,1\rangle$, $|b_1,1\rangle$, and $|p_+,0\rangle$. In both figures, the energy origin is taken at the $|s,0\rangle$ level.

discrete level $|p_-,0\rangle$ and the continuum $|s,1\rangle$ (Fig. 5). In the framework of the dispersionless phonon model, we demonstrate (see Appendix B) that this interaction reduces to the one between two discrete levels that gives rise to two discrete polarons noted $|a_1\rangle$ and $|b_1\rangle$. The energies of these two polarons are reported as solid lines in Fig. 6(a) for sample (II). Second, we study the two anticrossings at 70–80 meV, which involve the discrete level $|p_+,0\rangle$ and the continuums $|p_-,1\rangle$ and $|s,2\rangle$ (Fig. 5). In a first step, we have to consider the interaction between $|p_-,1\rangle$ and $|s,2\rangle$. We demonstrate in Appendix B that it gives rise to two flat polaron continuums: $|a_1,1\rangle$ and $|b_1,1\rangle$, whose energies are the same as in Fig. 6(a) shifted by $\hbar\omega_{LO}$ and are reported as dashed-dotted lines in Fig. 6(b). In a second step, we consider the interaction of the discrete level $|p_+,0\rangle$ with $|a_1,1\rangle$ and $|b_1,1\rangle$ continuums. The problem reduces to that of a three levels system (see Appendix B), the result being reported as solid lines in Fig. 6(b) for sample (II). Note that the Fröhlich Hamiltonian couples $|p_+,0\rangle$ to the $|p_-,1\rangle$ part of the $|a_1,1\rangle$ and $|b_1,1\rangle$ polarons only, since no direct interaction can take place between $|p_+,0\rangle$ and $|s,2\rangle$. This explains the small amplitude of the anticrossing between $|p_+,0\rangle$ and $|b_1,1\rangle$ around 16 T: the weight of $|p_-,1\rangle$ is much smaller than the weight of $|s,2\rangle$ in $|b_1,1\rangle$ at this magnetic field. One can check that the solid

(a)

(b)
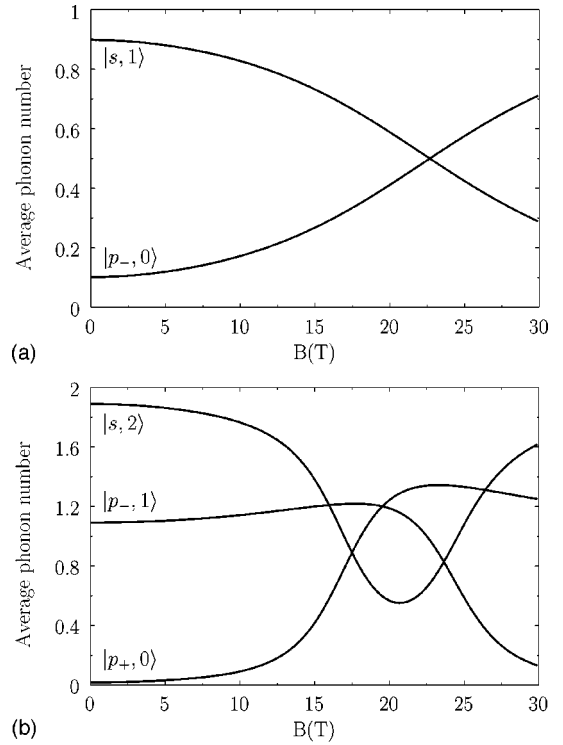
FIG. 7. Calculated average number $\bar{N}_i$ of LO phonons in the polaron eigenstates shown (a) in Fig. 6(a), and (b) in Fig. 6(b). The labels give the dominant component of the $B=0$ polaron states.

lines in Figs. 6(a) and 6(b) account very well for the experimental data. Moreover, using this dispersionless phonon model, we have calculated the average number of LO phonons at T=0 in each relevant polaron eigenstate $|\phi_i\rangle$, $\bar{N}_i = \langle\phi_i|\Sigma_q a_q^+ a_q|\phi_i\rangle$. The average number of phonons vs magnetic field is reported in Figs. 7(a) and 7(b). Around 40 meV [Fig. 7(a)], the eigenstates are linear combinations of the $|p_-,0\rangle$ and $|s,1\rangle$ states. At 70–80 meV [Fig. 7(b)], the eigenstates are linear combinations of the $|p_+,0\rangle$, $|p_-,1\rangle$, and $|s,2\rangle$ states. In the anticrossing regions, one can note the strong mixing between the noninteracting electron-phonon states. In addition, at low magnetic field, the number of phonons is not exactly 0, 1 or 2 showing that there is a mixing of the noninteracting electron-phonon states by the Fröhlich interaction even at $B=0$.

Finally, it is useful to discuss the time dependence of the survival probability for the various noninteracting electron-phonon states. In three-dimensional (3D) or 2D structures, the mixed electron-phonon states form a broad continuum, essentially because of the very large continuum of the conduction electronic states (~ 1 eV). The electron-phonon system prepared at $t=0$ in a factorized state, for example, $|\mathbf{k},0\rangle$ where $\mathbf{k}$ is the wave vector related to the free motion of the electron, is found to irreversibly dissolve in the continuum of the available final states $|\mathbf{k}',1_\mathbf{q}\rangle$ with $\mathbf{k}=\mathbf{k}'+\mathbf{q}$. The survival probability of still finding the electron-phonon system at t in the initial state $|\mathbf{k},0\rangle$ decreases exponentially.[17] This situation corresponds to a weak coupling regime to the extent that there is no way to form bound states between the delocalized
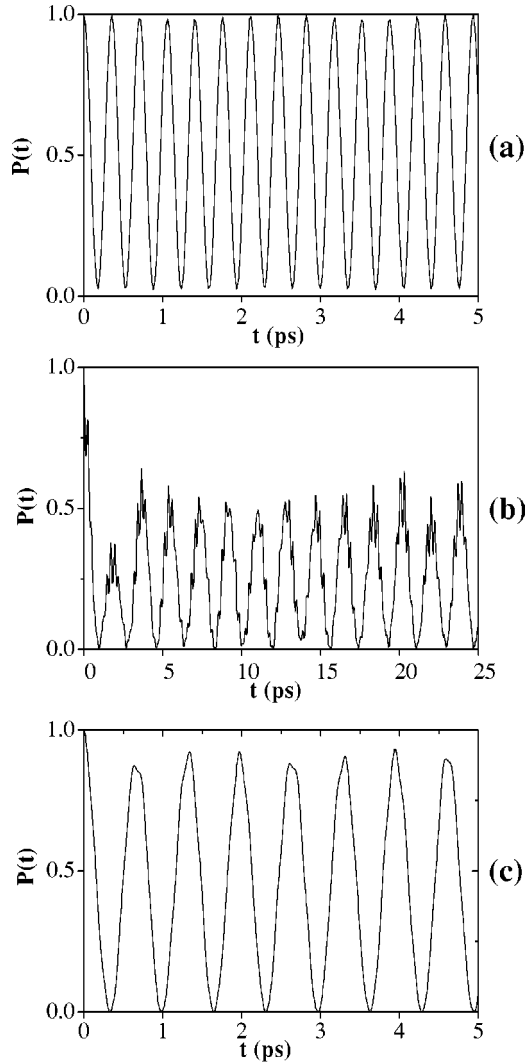
Figure 8

FIG. 8. Calculated time dependence in sample (III) of the survival probability (a) in the $|p_-,0\rangle$ level at $B=28$ T, (b) in the $|p_+,0\rangle$ level at $B=14$ T and (c) in the $|p_+,0\rangle$ level at $B=21$ T. These values of the magnetic field correspond to the various anticrossings.

electrons and the delocalized phonons. A completely different situation appears for QD's that display discrete electronic levels. For instance Fig. 8 shows such calculations for the various anticrossings observed in sample (III). The time dependences of the survival probability in the $|p_+,0\rangle$ level at $B=14$ T and 21 T and in the level $|p_-,0\rangle$ at 28 T are represented. One can see that the survival probability of an initial electron-phonon state with zero phonon never shows an exponential decay. It oscillates between 0 and 1 (or close to 1) in the case of one phonon polarons and between 0 and P_m <1 for the two phonon polarons. Such oscillations are similar to the well-known Rabi oscillations and would be everlasting if the polarons were stable. This would imply a strict impossibility for electrons to emit LO phonons. This effect is another indication that electrons and LO phonons behave very differently in QD's than in bulks or quantum-well structures, in particular, that they are in a strong coupling regime in QD's.

V. CONCLUSION

To summarize, we have investigated the FIR magneto-optical transitions in self-assembled InAs QD's with different lateral diameters and we have shown that a model neglecting the electron-phonon coupling is definitely unable to account for the experimental data. We have calculated the coupling between the relevant mixed electron-lattice states using the Fröhlich Hamiltonian and we have determined the polaron states as well as the energies of the dipolar electric transitions. We believe that the excellent agreement between the experiments and the calculations obtained for all the samples provides strong evidence that the magneto-optical transitions occur between polaron states and that the electrons and LO phonons experience a strong coupling regime in QD's.

The strong coupling regime raises the question of the energy relaxation in these systems since the usual relaxation channel, the irreversible emission of LO phonons by electrons, does not exist in quantum dots. Actually, the polaron states are genuinely unstable. The LO-phonon instability, due to crystal anharmonicity,[18] triggers the polaron decay. The various time constants involved in the population and coherence relaxation of a polaron by means of its coupling to the phonon thermostat through the anharmonicity effects have been recently calculated.[19] However, more theoretical and experimental investigations are necessary to fully understand energy loss rates in quantum dots.

APPENDIX A: ABSORPTION PROBABILITY OF THE *S-P* RESONANCE

For N_d dipoles (a dipole describes an electron in a dot) uniformly distributed on a plane of area S, the classical susceptibility is

$$\chi(\omega)=\frac{N_d e^2}{\varepsilon_0 m^* S}\left(\frac{1}{\omega_{sp}^2-\omega^2-\frac{i\omega}{\tau}}\right), \qquad (A1)$$

where ω_{sp} is the zero-field s-p resonant frequency and $1/\tau$ is the homogeneous damping. In the limit of small absorptions and near resonance the absorption probability reads

$$A(\omega)=\text{Im}[\chi(\omega)]\frac{\omega}{nc}, \qquad (A2)$$

where n is the refractive index and c is the light velocity. Because of the size dispersion of the QD's, ω_{sp} varies from one dot to another and one has to average $A(\omega)$ using a Gaussian probability density $P(\omega)$,

$$\bar{A} = \int_0^{+\infty} d\omega' P(\omega') A(\omega')$$

$$\text{with } P(\omega') = \frac{1}{\sigma\sqrt{2\pi}} \exp\left[-\frac{(\omega'-\bar{\omega})^2}{2\sigma^2}\right], \quad \text{(A3)}$$

where ω' is the resonance frequency of each dot, σ is the root-mean-squared deviation of the probability density, and $\bar{\omega}$ is the peak resonance frequency. Note that the homogeneous broadening $1/\tau \ll \sigma$ because τ is of the order of several microseconds (limited by the radiative recombination) and $\hbar\sigma$ is of the order of a few meV. In the limit $1/\tau \ll \sigma$, we find that

$$\bar{A}(\omega) = \bar{A}(\bar{\omega}) \exp\left[-\frac{(\omega-\bar{\omega})^2}{2\sigma^2}\right]$$

$$\text{with } \bar{A}(\bar{\omega}) = \frac{N_d}{S} \frac{e^2\pi}{2nc\varepsilon_0 m^*\sigma\sqrt{2\pi}}, \quad \text{(A4)}$$

σ is related to the width at half amplitude of the s-p resonance $\Delta = 4$ meV by $\sigma = \Delta/2\hbar\sqrt{2\ln 2}$. Taking $m^* = 0.07m_0$, $n = 3.52$, and $N_d = 4\times10^{10}$ cm^{-2} (one electron per dot), we find $\bar{A}(\bar{\omega}) = 0.44\%$. Note that the quantum model would give $\bar{A}_{qu}(\bar{\omega}) = \bar{A}(\bar{\omega}) \times f_{s\text{-}p}$ where $f_{s\text{-}p}$ is the oscillator strength of the s-p transition, but for our samples, we have calculated $f_{s\text{-}p} \approx 1$.[20]

APPENDIX B: INTERACTION BETWEEN DISCRETE LEVELS AND FLAT CONTINUUMS

In order to understand the origin and the amplitude of the various anticrossings observed in Fig. 4, we develop a simple model that involves dispersionless LO phonons. We deal with the Fröhlich-coupled discrete electronic levels $|s,0\rangle$, $|p_-,0\rangle$, and $|p_+,0\rangle$, and flat continuums $|s,1\rangle$, $|p_-,1\rangle$, $|s,2\rangle$, ... The Fröhlich term of the Hamiltonian writes

$$H_{int} = \sum_{\mathbf{q}} \{V(q) a_{\mathbf{q}}^+ + V^*(q) a_{\mathbf{q}}\}. \quad \text{(B1)}$$

First, we consider the interaction between one discrete level, say $|p_-,0\rangle$, and the one-phonon continuum $|s,1\rangle$. We note $V_{sp_-}(\mathbf{q}) = \langle s,1_{\mathbf{q}}|H_{int}|p_-,0\rangle$. We perform linear combinations of the degenerate one-phonon states $|1_{\mathbf{q}}\rangle$ and introduce a particular linear combination,

$$|1_{\alpha(sp_-)}\rangle = \frac{\sum\limits_{\mathbf{q}} V_{sp_-}(\mathbf{q})|1_{\mathbf{q}}\rangle}{\sqrt{\sum\limits_{\mathbf{q}} |V_{sp_-}(\mathbf{q})|^2}}, \quad \text{(B2)}$$

$$\langle s,1_{\alpha(sp_-)}|H_{int}|p_-,0\rangle = \sqrt{\sum_{\mathbf{q}} |V_{sp_-}(\mathbf{q})|^2} = V_{\text{eff}}(sp_-). \tag{B3}$$

We label $|1_\beta\rangle$ the remaining one-phonon combinations orthogonal to $|1_{\alpha(sp_-)}\rangle$. Thus, by construction, we have

$$\langle s,1_\beta|H_{int}|p_-,0\rangle = 0. \tag{B4}$$

Therefore, the $|p_-,0\rangle$ level is coupled only to a single state of the continuum: $|s,1_{\alpha(sp_-)}\rangle$, while the other continuum levels $|s,1_\beta\rangle$ remain uncoupled to it. We have in this way an interaction between two discrete levels that gives rise to two polarons, noted $|a_1\rangle$ and $|b_1\rangle$, with an anticrossing energy of $2V_{\text{eff}}(sp_-)$. These polarons are a mixture of $|p_-,0\rangle$ and $|s,1_{\alpha(sp_-)}\rangle$. We can now generalize this procedure to handle the interactions between several mutually orthogonal discrete zero phonon levels and several flat continuums with one LO phonon: each discrete level is coupled to only one particular linear combination of each continuum. So if we have N discrete levels and M continuums, we need only to consider $N \times (M+1)$ levels.

In order to describe the two anticrossings observed in Fig. 4 at 70–80 meV, we also include interactions with the two flat continuums $|p_-,1_\mathbf{q}\rangle$ and $|s,2_{\mathbf{q}\mathbf{q}'}\rangle$. By combining the one phonon states $|1_{\alpha(sp_-)}\rangle$ and $|1_\beta\rangle$ defined above, we can form the two phonons levels $|2_{\nu\mu}\rangle$ with $(\nu,\mu) = [\alpha(sp_-),\alpha(sp_-)]$, $[\alpha(sp_-),\beta]$ or (β,β'). We have then

$$\langle s,2_{\beta\beta'}|H_{int}|p_-,1_{\beta''}\rangle = 0,$$

$$\langle s,2_{\alpha(sp_-)\beta}|H_{int}|p_-,1_{\beta'}\rangle = \delta_{\beta,\beta'} V_{\text{eff}}(sp_-), \tag{B5}$$

$$\langle s,2_{\alpha(sp_-)\alpha(sp_-)}|H_{int}|p_-,1_{\alpha(sp_-)}\rangle = V_{\text{eff}}(sp_-)\sqrt{2}.$$

Thus, we see that the set of two-phonons states $|s,2_{\beta\beta'}\rangle$ remains uncoupled, that each level of the one-phonon set $|p_-,1_\beta\rangle$ leads to a two levels system with $|s,2_{\alpha(sp_-)\beta}\rangle$ [with the same anticrossing energy $2V_{\text{eff}}(sp_-)$ as before] and that $|p_-,1_{\alpha(sp_-)}\rangle$ interacts with $|s,2_{\alpha(sp_-)\alpha(sp_-)}\rangle$ [anticrossing energy of $2\sqrt{2}V_{\text{eff}}(sp_-)$]. In summary, we end up with a two-phonon unperturbed continuum $|s,2\rangle$, two flat polaron continuums $|a_1,1_\beta\rangle$ and $|b_1,1_\beta\rangle$ (whose energies are the same as those of $|a_1\rangle$ and $|b_1\rangle$ shifted by $\hbar\omega_{LO}$), and two discrete polaron levels $|a_2\rangle$ and $|b_2\rangle$. These two last discrete polaron levels are not observed experimentally because light couples only levels involving the same number of phonons.

We can now add to the basis the discrete level $|p_+,0\rangle$. This later will be brought in resonance with $|s,2_{\beta\beta'}\rangle$, $|a_1,1_\beta\rangle$, $|b_1,1_\beta\rangle$, $|a_2\rangle$, and $|b_2\rangle$ states when the magnetic field varies. We note, however, that $\langle p_+,0|H_{int}|s,2_{\beta\beta'}\rangle = 0$ because the Fröhlich term does not couple states differing by two phonons. Also, we can show that $\langle p_+,0|H_{int}|a_2$ or $b_2\rangle \sim \langle p_+,0|H_{int}|p_-,1_{\alpha(sp_-)}\rangle \sim \Sigma_\mathbf{q} V_{p_+p_-}(\mathbf{q}) V_{sp_-}^*(\mathbf{q}) = 0$ [where

$V_{p_+p_-}(\mathbf{q})$ is defined similarly to $V_{sp_-}(\mathbf{q})$]. The interactions with $|a_1,1_\beta\rangle$ or $|b_1,1_\beta\rangle$ do not vanish and are proportional to $\langle p_+,0|H_{int}|p_-,1_\beta\rangle$. Following the procedure described above, we can perform linear combinations of the degenerate phonon levels $|1_\mathbf{q}\rangle$ to introduce, in addition to the particular combination $|1_{\alpha(sp_-)}\rangle$, another (orthogonal) particular combination $|1_{\alpha(p_+p_-)}\rangle$. It turns out that the levels $|a_1,1_{\alpha(p_+p_-)}\rangle$ or $|b_1,1_{\alpha(p_+p_-)}\rangle$ are the only ones that are coupled to $|p_+,0\rangle$. Similarly to $V_{eff}(sp_-)$, we define an effective coupling $V_{eff}(p_+p_-)$. As a consequence, we simplify the problem to a three levels system: $|p_+,0\rangle$, $|a_1,1_{\alpha(p_+p_-)}\rangle$, and $|b_1,1_{\alpha(p_+p_-)}\rangle$. The Hamiltonian of this reduced system is given by

$$\begin{pmatrix} E_{|p_+,0\rangle} & u_a V_{eff}(p_+p_-) & u_b V_{eff}(p_+p_-) \\ u_a V_{eff}(p_+p_-) & E_{|a_1\rangle}+\hbar\omega_{LO} & 0 \\ u_b V_{eff}(p_+p_-) & 0 & E_{|b_1\rangle}+\hbar\omega_{LO} \end{pmatrix},$$

(B6)

where $u_a=\langle a_1|p_-,0\rangle$ and $u_b=\langle b_1|p_-,0\rangle$, $E_{|p_+,0\rangle}$, $E_{|a_1\rangle}$, and $E_{|b_1\rangle}$ are the energies of the levels $|p_+,0\rangle$, $|a_1\rangle$, and $|b_1\rangle$, respectively.

These calculations are valid only if the amplitudes of the anticrossings are much larger than the widths of the continuums. This is actually the case for the samples we have studied, since there is $V_{eff}(sp_-)\sim 4.5$ meV and $V_{eff}(p_+p_-)\sim 3.7$ meV.

[1] U. Bockelmann and G. Bastard, Phys. Rev. B **42**, 8947 (1990).

[2] T. Inoshita and H. Sakaki, Phys. Rev. B **56**, R4355 (1997).

[3] S. Hameau, Y. Guldner, O. Verzelen, R. Ferreira, J. Zeman, A. Lemaître, and J.M. Gérard, Phys. Rev. Lett. **83**, 4152 (1999).

[4] L. Goldstein, F. Glas, J.Y. Marzin, M.N. Charasse, and G. Leroux, Appl. Phys. Lett. **47**, 1099 (1985).

[5] M. Fricke, A. Lorke, J.P. Kotthaus, G. Medeiros-Ribeiro, and P.M. Petroff, Europhys. Lett. **36**, 197 (1996).

[6] Y. Hasegawa, H. Kiyama, Q.K. Xue, and T. Sakurai, Appl. Phys. Lett. **72**, 2265 (1998).

[7] Y. Nabetani, T. Ishikawa, S. Noda, and A. Sasaki, J. Appl. Phys. **76**, 347 (1994).

[8] B. Grandidier, Y.M. Niquet, B. Legrand, J.P. Nys, C. Priester, D. Stiévenard, J.M. Gérard, and V. Thierry-Mieg, Phys. Rev. Lett. **85**, 1068 (2000).

[9] P.W. Fry, I.E. Itskevich, D.J. Mowbray, M.S. Skolnick, J.J. Finley, J.A. Barker, E.P. O'Reilly, L.R. Wilson, I.A. Larkin, P.A. Maksym, M. Hopkinson, M. Al-Khafaji, J.P.R. David, A.G. Cullis, G. Hill and J.C. Clark, Phys. Rev. Lett. **84**, 733 (2000).

[10] P.B. Joyce, T.J. Krzyzewski, G.R. Bell, B.A. Joyce, and T.S. Jones, Phys. Rev. B **58**, R15 981 (1998).

[11] P.D. Wang, N.N. Ledentsov, C.M. Sotomayor-Torres, I.N. Yassievich, A. Pakhomov, A.Yu. Egovov, P.S. Kop'ev, and V.M. Ustinov, Phys. Rev. B **50**, 1604 (1994).

[12] C. R. Pidgeon, in *Handbook on Semiconductors*, edited by M. Balkanski (North-Holland Publishing Company, Amsterdam, 1980), Vol. 2, p. 270, and references therein.

[13] E.J. Johnson and D.M. Larsen, Phys. Rev. Lett. **16**, 655 (1966).

[14] Y. J. Wang, H. A. Nickel, B. D. McCombe, F. M. Peeters, G. Q. Hai, J. M. Shi, J. T. Devreesse, and X. G. Wu, in *High Magnetic Field in the Physics of Semiconductors II*, edited by G. Landwehr and W. Ossau (World Scientific Publishing Company, Singapore, 1997), Vol. 2, p. 797.

[15] X.Q. Li and Y. Arakawa, Phys. Rev. B **57**, 12 285 (1998).

[16] R. Heitz, M. Veit, N.N. Ledentsov, A. Hoffmann, D. Bimberg, V.M. Ustinov, P.S. Kop'ev, and Zh.I. Alferov, Phys. Rev. B **56**, 10 435 (1997).

[17] C. Kittel, *Quantum Theory of Solids* (Wiley, New York).

[18] F. Vallée and F. Bogani, Phys. Rev. B **43**, 12 049 (1991); F. Vallée, *ibid.* **49**, 2460 (1994).

[19] O. Verzelen, R. Ferreira, and G. Bastard, Phys. Rev. B **62**, R4809 (2000).

[20] A. Vasanelli, M. De Giorgi, R. Ferreira, R. Cingolani, and G. Bastard, Physica E (to be published).